LETTER

doi:10.1038/nature11246

How atomic nuclei cluster

J.-P. Ebran[1], E. Khan[2], T. Nikšić[3] & D. Vretenar[3]

Nucleonic matter displays a quantum-liquid structure, but in some cases finite nuclei behave like molecules composed of clusters of protons and neutrons. Clustering is a recurrent feature in light nuclei, from beryllium to nickel[1–3]. Cluster structures are typically observed as excited states close to the corresponding decay threshold; the origin of this phenomenon lies in the effective nuclear interaction, but the detailed mechanism of clustering in nuclei has not yet been fully understood. Here we use the theoretical framework of energy-density functionals[4,5], encompassing both cluster and quantum liquid-drop aspects of nuclei, to show that conditions for cluster formation can in part be traced back to the depth of the confining nuclear potential. For the illustrative example of neon-20, we show that the depth of the potential determines the energy spacings between single-nucleon orbitals in deformed nuclei, the localization of the corresponding wavefunctions and, therefore, the degree of nucleonic density clustering. Relativistic functionals, in particular, are characterized by deep single-nucleon potentials. When compared to non-relativistic functionals that yield similar ground-state properties (binding energy, deformation, radii), they predict the occurrence of much more pronounced cluster structures. More generally, clustering is considered as a transitional phenomenon between crystalline and quantum-liquid phases of fermionic systems.

The occurrence of molecular states in atomic nuclei and the formation of clusters of nucleons were predicted in the 1930s (refs 1 and 2). Subsequently, the description of nuclear dynamics came to be based predominantly on the concept of independent nucleons in a mean-field potential, but a renewed interest in clustering phenomena in the 1960s led to the development of theoretical methods dedicated to considering clusters[3]. Numerous experimental studies have revealed a wealth of data on clustering phenomena in light nuclei[3], and modern theoretical approaches use microscopic models that take single-nucleon degrees of freedom fully into account[6–8]. Clustering gives rise to nuclear molecules. For instance, in ^{12}C the second 0^+ state—the Hoyle state that has a key role in stellar nucleosynthesis—is predicted to display a structure composed of three α-particles[9,10]. The binding energy of the α-particle, formed from two protons and two neutrons, is much larger than that of other light nuclei. Cluster radioactivity[11], discovered in the 1980s, is another manifestation of clustering in atomic nuclei. Experimental signatures of clustering are usually indirect. Quasi-molecular resonances are probed by scattering one cluster on another, such as in the ^{12}C+^{12}C system[3,12], and cluster structures are also discernible in the break-up of nuclei. Evidence has been reported for the formation of clusters in ground and excited states of a number of α-conjugate nuclei[3]; that is, nuclei with an equal, even number of protons and neutrons, from ^{8}Be to ^{56}Ni.

The mechanism of cluster formation has not yet been fully understood. As shown in Ikeda diagrams[13], cluster structures are predicted to appear as excited states close to the corresponding decay threshold. However, the origin of cluster formation lies in the effective nuclear interaction, and signatures should also be present in the ground state[14–16]. Deformation has an important role because it removes the degeneracy of single-nucleon levels associated with spherical symmetry. At specific deformations the shell structure can restore degeneracies corresponding, for instance, to a 2:1 ratio of the large axis over the small axis of a quadrupole deformed system[3]. Consequently, the restored degeneracy of deformed shell closures facilitates the formation of clusters. However, this may be a rather qualitative explanation, because clustering phenomena cannot generally be explained by accidental degeneracies. Clustering is an essential feature of many-nucleon dynamics that coexists with the nuclear mean-field. Therefore, although in most cluster models the existence of such structures is assumed a priori and the corresponding effective interactions are adjusted to the binding energies and scattering phase shifts of these configurations, a fully microscopic understanding of cluster formation necessitates a more general description that encompasses both cluster and quantum liquid-drop aspects in light and heavier nuclei. It is well known that deformation and closeness to the cluster-emission threshold favour cluster formation. States close to the particle-emission threshold cannot be isolated from the environment of scattering states, so cluster states at the threshold belong to an open quantum system[17]. The aim of this work is to further explore the origin of clustering: to examine the conditions for cluster formation in ground states of finite nuclei, starting from a fully microscopic description based on the framework of energy-density functionals (EDFs).

At present, the only comprehensive approach to nuclear structure is based on the framework of EDFs. Nuclear EDFs enable a complete and accurate description of ground-state properties and collective excitations over the whole nuclide chart[4,5]. In practical implementations, nuclear EDFs are analogous to Kohn−Sham Density Functional Theory, the most widely used method for electronic-structure calculations in condensed-matter physics and quantum chemistry. In the nuclear case, the many-body dynamics is represented by independent nucleons moving in a local self-consistent mean-field potential that corresponds to the actual density and current distribution of a given nucleus. Both relativistic and non-relativistic realizations of EDFs are used in studies of nuclear matter and finite nuclei. A nuclear EDF is universal in the sense that, for a given inter-nucleon interaction, it has the same functional form for all systems. Using a small set of global parameters adjusted to empirical properties of homogeneous nuclear matter and data on finite nuclei, a universal functional provides a description of the structure of nuclei across the chart of nuclides.

A number of recent studies based on nuclear EDFs or the mean-field approach have analysed cluster structures in α-conjugate nuclei[14–16,18–20]. In Fig. 1 we display the self-consistent ground-state densities of ^{20}Ne, calculated with two widely used functionals that are representative of the two classes of nuclear EDFs: the non-relativistic Skyrme SLy4 (ref. 21), and the relativistic functional DD-ME2 (ref. 22). The equilibrium shape of ^{20}Ne is a prolate, axially symmetric quadrupole ellipsoid. Although they have not been specifically adjusted to this mass region, both functionals reproduce the empirical ground-state properties of this nucleus: the experimental binding energy, 160.6 MeV; the radius of the proton distribution, 2.90 fm (ref. 23); and the radius of the matter distribution, 2.85 fm (ref. 24), all with a typical accuracy to within roughly 1%. It is remarkable that, although these functionals predict similar values for the binding energy, charge and matter radii, and quadrupole deformation

[1]CEA/DAM/DIF, F-91297 Arpajon, France. [2]Institut de Physique Nucléaire, Université Paris-Sud, IN2P3-CNRS, F-91406 Orsay Cedex, France. [3]Physics Department, Faculty of Science, University of Zagreb, 10000 Zagreb, Croatia.

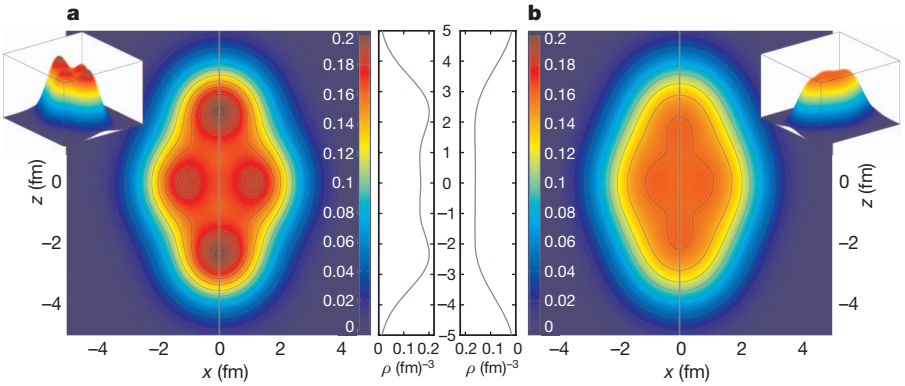

Figure 1 | Self-consistent ground-state densities of ^{20}Ne. Two nuclear energy-density functionals are used: **a**, DD-ME2 (ref. 22), and **b**, Skyrme SLy4 (refs 21 and 30). The densities (in units of fm^{-3}) are plotted in the $x-z$ plane of the intrinsic frame of reference that coincides with the principal axes of the nucleus, with z chosen as the symmetry axis. The inserts show the corresponding three-dimensional density plots and the density profiles (ρ) along the symmetry axis ($x = 0$).

of the equilibrium shape of ^{20}Ne, the corresponding single-nucleon densities are qualitatively very different. The density calculated with SLy4 displays a smooth behaviour characteristic of a Fermi liquid, with an extended surface region in which the density very gradually decreases from the central value of around 0.16 fm^{-3} (Fig. 1b). The relativistic functional DD-ME2, on the other hand, predicts an equilibrium density that is much more localized. The formation of cluster structures is clearly visible, with density spikes as large as roughly 0.2 fm^{-3}, and a much narrower surface region (Fig. 1a).

Understanding the difference in the equilibrium densities of ^{20}Ne calculated with SLy4 and DD-ME2 is a key to the mechanism of ground-state cluster formation in this mass region of α-conjugate deformed nuclei. The axially symmetric deformation of the nuclear mean-field removes the degeneracy of spherical single-nucleon levels, and nucleons paired by spin (up and down) occupy orbitals characterized by time-reversal degeneracy. For large deformations these levels can be labelled by a set of asymptotic Nilsson quantum numbers[25] and, because of the relatively weak Coulomb interactions in light nuclei, the localization of proton and neutron orbitals is similar in nuclei with equal numbers of protons and neutrons ($Z = N$ nuclei). In the specific case of ^{20}Ne, ten protons and ten neutrons occupy five deformed Nilsson levels, with the energy spacing between these levels proportional to the deformation of the single-nucleon potential. Figure 2 shows the partial single-nucleon densities that correspond to the highest occupied Nilsson orbital. Even without introducing a quantitative measure of localization, it is obvious that DD-ME2 predicts a much more localized density distribution (Fig. 2a). More-localized density distributions are also obtained for the other four occupied orbitals when calculated using DD-ME2.

Localization of densities that correspond to single-particle orbitals is a necessary precondition for the formation of clusters, and this effect can be traced back to the corresponding single-nucleon spectra. The comparison of spectra calculated with the two functionals shows that the one obtained with DD-ME2 is more spread out, and the more pronounced energy spacings between single-particle levels are also reflected in the more localized wavefunctions and partial densities. Starting from degenerate spherical single-particle levels, the splitting of the corresponding Nilsson deformed states is proportional to the deformation, and to the depth of the potential. Given that the two functionals predict almost identical equilibrium deformations and radii for ^{20}Ne, the different energy spacings in the single-nucleon spectra must have their origin in the difference in the corresponding potentials. In fact, the self-consistent mean-field potential of DD-ME2 is considerably deeper than that of SLy4. In the centre of the nucleus, the depth of the DD-ME2 single-neutron potential is −78.6 MeV, whereas the depth of the SLy4 potential is −69.5 MeV. The corresponding values of the single-proton potentials are −72.8 MeV for DD-ME2 and −64.6 MeV for SLy4. The effect of the potential depth on the localization of wavefunctions is shown schematically in Fig. 3a, where, as an approximation to nuclear potentials, we plot three harmonic-oscillator potentials with different depth values—30, 45 and 60 MeV—but the same radius, $R = 3$ fm. The radial wavefunctions of the corresponding p-states are shown in Fig. 3b. The oscillator length b determines the position of the maximum and the dispersion of the wavefunction[26]. The deeper the potential, the smaller the oscillator length (see the expression in the legend of Fig. 4), and the more localized the wavefunctions. In the classically forbidden region ($R > 3$ fm on Fig. 3), a smaller oscillator length leads to a more rapid

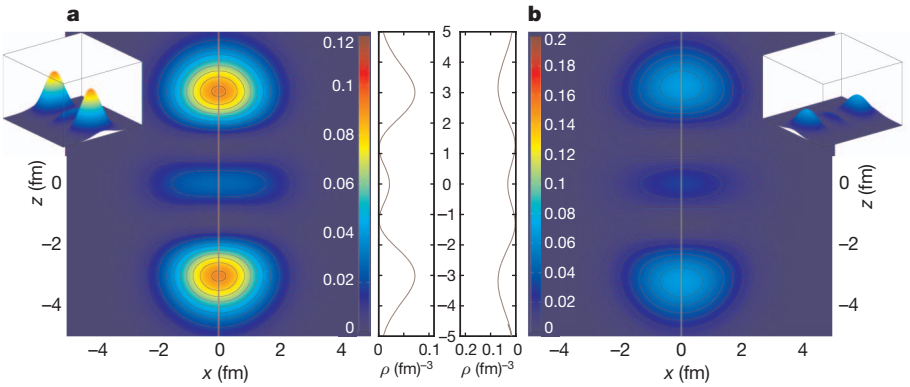

Figure 2 | Partial nucleon density distributions. Density distributions that correspond to the highest occupied level (2 protons spin up and down, and 2 neutrons spin up and down) in ^{20}Ne, having Nilsson quantum numbers $1/2^{+}[220]$, calculated using the nuclear energy-density functionals DD-ME2 (ref. 22) (**a**) and SLy4 (refs 21 and 30) (**b**).

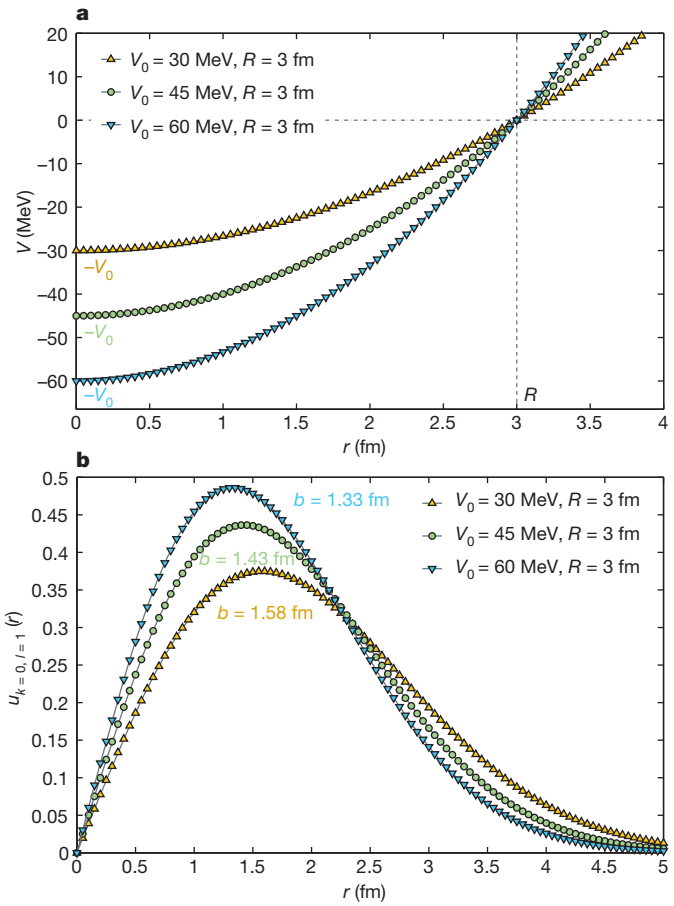

Figure 3 | Harmonic oscillators of different depths. **a**, Potentials plotted against the radial coordinate r for harmonic oscillators with the same radius, $R = 3$ fm, and depths (V_0) of 30, 45 and 60 MeV. **b**, The radial wavefunctions $U_{k,l}$ of the corresponding first p-state, where k is the radial quantum number and l the azimuthal one. The position of the maximum is determined by the oscillator length b.

exponential decay of the wavefunction, also favouring its localization. Hence a larger depth of the potential leads to a more pronounced localization of the wavefunction, in both the classically allowed and the forbidden regions, as shown in Fig. 3. In the present study we have verified, through a series of self-consistent mean-field calculations using a variety of non-relativistic and relativistic functionals for ^{20}Ne, ^{24}Mg, ^{28}Si and ^{32}S, that pronounced cluster structures in deformed equilibrium shapes indeed occur only for deep single-nucleon potentials.

The difference between the potential depths calculated with DD-ME2 and SLy4 is characteristic for relativistic versus non-relativistic self-consistent potentials. The depth of a relativistic potential is determined by the difference between two large fields: an attractive (negative) Lorentz scalar potential of magnitude around 400 MeV, and a repulsive Lorentz vector potential of roughly 320 MeV (plus the repulsive Coulomb potential for protons)[4,5]. In uniform matter these potentials are determined by the choice of the nuclear-matter equation of state; that is, by the density at which nucleonic matter saturates and by the binding energy per nucleon at saturation. The corresponding scalar and vector nucleon densities are related by a self-consistency condition[27] (in infinite matter the potentials are constant and proportional to the corresponding densities). Moreover, the sum of these potentials (about 700 MeV) determines the effective single-nucleon spin–orbit force in finite nuclear systems, which naturally manifests itself with the empirical strength. In a non-relativistic approach the spin–orbit potential is included in a purely phenomenological way, with the strength of the interaction adjusted to empirical energy spacings

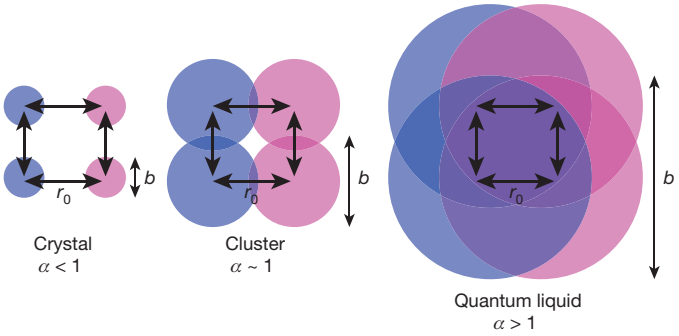

Figure 4 | Schematic illustration of the transition from a crystalline to a quantum liquid phase, including the cluster phase. The dimensionless parameter $\alpha = b/r_0$, where b is the dispersion of the fermion wavefunction and r_0 the typical inter-fermion distance, quantifies nuclear clustering. For a harmonic oscillator $\alpha = (\hbar R)^{1/2}\,(2mV_0)^{-1/4}\,r_0^{-1}$, where V_0 is the depth of the potential, R the radius of the system, m the mass of the nucleon and $\hbar$ Planck's constant/2π.

between spin–orbit partner states. Because the relativistic scalar and vector fields determine both the effective spin–orbit potential and the self-consistent single-nucleon mean-field, the latter is found to be deeper than the non-relativistic mean-field potentials for all relativistic functionals.

More generally, fermionic systems can exhibit a crystalline phase or, on the other extreme, a quantum liquid phase. The 'quantality' parameter has been thought[28] to show that nuclear matter displays a quantum-liquid structure. This concept can be generalized by considering nuclear clusters as transitional states between crystalline and quantum-liquid phases (Fig. 4). The dimensionless ratio $\alpha = b/r_0$, where b is the dispersion of the nucleon wavefunction and r_0 is the typical inter-nucleon distance (roughly 1.2 fm), is the natural parameter to quantify nuclear clustering, in analogy with similar considerations in condensed matter[29]. When α is greater than 1, nucleons are delocalized and the nucleus has a quantum-liquid structure. The transition to a cluster state occurs when α is about 1, so that nucleons become more localized and form a molecular structure (Fig. 4). In the present analysis we find that α is smaller than 1 for the relativistic functional, whereas it is greater than 1 for the non-relativistic functional. Moreover, from its definition in the case of a harmonic-oscillator potential (see legend of Fig. 4), α obviously increases with the number of nucleons (nuclear radius). Cluster states, therefore, are less likely to appear in heavier nuclei. The present discussion is also relevant for studies of the 'pasta' phase (located between the Wigner crystal and nuclear-matter phases) in the crust of neutron stars.

Received 6 March; accepted 17 May 2012.

1. Weizsäcker, C. F. V. Neuere Modellvorstellungen über den Bau der Atomkerne. *Naturwissenschaften* **26,** 209–217 (1938).
2. Wheeler, J. A. On the mathematical description of light nuclei by the method of resonating group structure. *Phys. Rev.* **52,** 1107–1122 (1937).
3. Von Oertzen, W. V., Freer, M. & Kanada-En'yo, Y. Nuclear clusters and nuclear molecules. *Phys. Rep.* **432,** 43–113 (2006).
4. Bender, M., Heenen, P.-H. & Reinhard, P.-G. Self-consistent mean-field models for nuclear structure. *Rev. Mod. Phys.* **75,** 121–180 (2003).
5. Vretenar, D., Afanasjev, A. V., Lalazissis, G. A. & Ring, P. Relativistic Hartree–Bogoliubov theory: static and dynamic aspects of exotic nuclear structure. *Phys. Rep.* **409,** 101–259 (2005).
6. Kanada-En'yo, Y. & Horiuchi, H. Structure of light unstable nuclei studied with antisymmetrized molecular dynamics. *Prog. Theor. Phys.* **142** (Suppl.), 205–263 (2001).
7. Feldmeier, H., Bieler, K. & Schnack, J. Fermionic molecular dynamics for ground states and collision of nuclei. *Nucl. Phys. A* **586,** 493–532 (1995).
8. Neff, T. & Feldmeier, H. Tensor correlations in the unitary correlation operator method. *Nucl. Phys. A* **713,** 311–371 (2003).
9. Tohsaki, A., Horiuchi, H., Schuck, P. & Röpke, G. Alpha cluster condensation in ^{12}C and ^{16}O. *Phys. Rev. Lett.* **87,** 192501 (2001).
10. Fynbo, H. O. U. *et al.* Revised rates for the stellar triple-α process from measurement of ^{12}C nuclear resonances. *Nature* **433,** 136–139 (2005).
11. Rose, H. J. & Jones, G. A. A new kind of natural radioactivity. *Nature* **307,** 245–247 (1984).
12. Greiner, W., Park, J. Y. & Scheid, W. *Nuclear Molecules* (World Scientific, 1995).

13. Ikeda K., Tagikawa N. & Horiuchi H.. The systematic structure-change into the molecule-like structures in the self-conjugate 4*n* nuclei. *Prog. Theor. Phys.* **464** (Suppl.), 464–475 (1968).
14. Arumugam, P., Sharma, B. K. & Patra, S. K. Relativistic mean field study of clustering in light nuclei. *Phys. Rev. C* **71,** 064308 (2005).
15. Maruhn, J. A. *et al.* α-Cluster structure and exotic states in a self-consistent model for light nuclei. *Phys. Rev. C* **74,** 044311 (2006).
16. Reinhard, P.-G., Maruhn, J. A., Umar, A. S. & Oberacker, V. E. Localization in light nuclei. *Phys. Rev. C* **83,** 034312 (2011).
17. Okolowicz, J., Ploszajczak, M. & Nazarewicz, W. On the origin of nuclear clustering. Preprint at ⟨http://arxiv.org/abs/1202.6290⟩ (2012).
18. Girod, M. & Grammaticos, B. Triaxial Hartree–Fock–Bogolyubov calculations with D1 effective interaction. *Phys. Rev. C* **27,** 2317–2339 (1983).
19. Ichikawa, T., Marhun, J. A., Itagaki, N. & Ohkubo, S. Linear chain structure of four-α clusters in ^{16}O. *Phys. Rev. Lett.* **107,** 112501 (2011).
20. Robledo, L. M. & Bertsch, G. F. Global systematics of octupole excitations in even–even nuclei. *Phys. Rev. C* **84,** 054302 (2011).
21. Chabanat, E., Bonche, P., Haensel, P., Meyer, J. & Schaeffer, R. A Skyrme parametrization from subnuclear to neutron star densities part II. Nuclei far from stabilities. *Nucl. Phys. A* **635,** 231–256 (1998).
22. Lalazissis, G. A., Nikšić, T., Vretenar, D. & Ring, P. New relativistic mean-field interaction with density-dependent meson-nucleons couplings. *Phys. Rev. C* **71,** 024312 (2005).
23. Fricke, G. *et al.* Behavior of the nuclear charge radii systematics in the *s-d* shell from muonic atom measurement. *Phys. Rev. C* **45,** 80–89 (1992).
24. Chulkov, L. *et al.* Interaction cross sections and matter radii of $A = 20$ isobars. *Nucl. Phys. A* **603,** 219–237 (1996).
25. Nilsson, S. G. Binding states of individual nucleons in strongly deformed nuclei *Mat. Fys. Medd. Dan. Vid. Selsk.* **29,** 1–69 (1955).
26. Cohen-Tannoudji, C., Diu, B. & Laloë, F. *Mécanique Quantique* (Hermann Ed., 1973).
27. Walecka, J. D. *Theoretical Nuclear and Subnuclear Physics* (Imperial College Press and World Scientific, 2004).
28. Mottelson, B. Elementary features of nuclear structure. In *Les Houches Session LXVI, Trends in Nuclear Physics, 100 Years Later* (eds Nifenecker, H., Blaizot, J.-P., Bertsch, G. F., Weise, W. & David, F.) 25–121 (North-Holland Elsevier, 1996).
29. Pines, D. & Nozières, P. *The theory of quantum liquids* (Benjamin, 1966).
30. Stoitsov, M. V., Dobaczewski, J., Nazarewicz, W. & Ring, P. Axially deformed solution of the Skyrme–Hartree–Fock–Bogolyubov equations using the transformed harmonic oscillator basis. The program HFBTHO (v1.66p). *Comput. Phys. Commun.* **167,** 43–63 (2005).

Acknowledgements This work was supported by the Institut Universitaire de France and by the Croatian Ministry of Science, Education and Sport—project 1191005-1010. The authors thank J. Margueron, M. Milin, T. Neff, N. Van Giai and P. Schuck for comments and suggestions.

Author Contributions Model calculations were done by J.-P.E., E.K., T.N. and D.V. The manuscript text was prepared by E.K. and D.V. with contributions from J.-P.E. and T.N. J.-P.E. and E.K. prepared the figures.

Author Information Reprints and permissions information is available at www.nature.com/reprints. The authors declare no competing financial interests. Readers are welcome to comment on the online version of this article at www.nature.com/nature. Correspondence and requests for materials should be addressed to E.K. (khan@ipno.in2p3.fr).